Monthly Notices
of the
ROYAL ASTRONOMICAL SOCIETY

MNRAS **444,** 2676–2684 (2014) doi:10.1093/mnras/stu1595

Parallel and perpendicular diffusion coefficients of energetic particles interacting with shear Alfvén waves

M. Hussein★ and A. Shalchi★

Department of Physics and Astronomy, University of Manitoba, Winnipeg, MB R3T 2N2, Canada

Accepted 2014 August 4. Received 2014 July 10; in original form 2014 April 25

ABSTRACT

We investigate the interaction of energetic particles with parallel propagating shear Alfvén waves. We use analytical tools as well as test-particle simulations. The analytical derivation of the parallel diffusion coefficient is done by employing quasi-linear theory, a well-known tool in diffusion theory. The perpendicular diffusion coefficient, however, is derived by employing the unifield non-linear transport theory. This is the first time we derive a simple analytical form of the perpendicular mean free path based on the latter theory. We perform the simulations and we show that quasi-linear theory works well for parallel diffusion in Alfvénic slab turbulence as expected. We also show that the unified non-linear transport theory perfectly describes perpendicular diffusion for the turbulence model used here.

Key words: Diffusion – magnetic fields – turbulence.

1 INTRODUCTION

The interaction of energetic particles with turbulence is a well-known problem in space science and astrophysics (see, e.g. Schlickeiser 2002; Shalchi 2009, for reviews). In such scenarios, electrically charged particles interact with large-scale magnetic fields such as the solar magnetic field or the Galactic magnetic field and turbulence. The latter interaction is complicated since turbulent fields scatter the particles and makes their motion a diffusive one (we like to point out that non-diffusive transport has been discussed more recently in the literature – see Perrone et al. 2013 for a review).

If the transport of particles is investigated theoretically, one can use two different tools, namely:

(i) *Analytical theories* such as quasi-linear theory (QLT; see, e.g. Jokipii 1966) or non-linear diffusion theories (see, e.g. Shalchi 2010).

(ii) *Test-particle simulations* (see, e.g. Michałek & Ostrowski 1996; Qin, Matthaeus & Bieber 2002; Tautz 2010a,b; Hussein & Shalchi 2014).

Both approaches have their advantages and disadvantages. In analytical theories, for instance, one has to use approximations to achieve analytical tractability. On the other hand, for applications one needs analytical forms of the diffusion coefficients. Examples for such applications are the acceleration of particles at interplanetary shocks (see Li et al. 2012; Wang, Qin & Zhang 2012) and solar modulation studies (see Alania et al. 2013; Engelbrecht & Burger 2013; Manuel, Ferreira & Potgieter 2014; Potgieter et al. 2014).

★E-mail: m_hussein@physics.umanitoba.ca (MH); andreasm4@yahoo.com (AS)

In both cases, analytical theory and numerical treatments of the transport, one has to specify the properties of magnetic turbulence which controls the motion of the energetic particles. One could say that three properties of turbulence are relevant for the transport. Those are:

(i) The *geometry* of the turbulence describing how the turbulent magnetic fields depend on the wave vector orientations. Simple examples for turbulence geometries are the slab model, the two-dimensional model, and the isotropic model.

(ii) The *turbulence spectrum* describes how the magnetic fields depend on the wavenumber or scale. Here, one usually employs a model with simple power laws in the different regimes (energy range, inertial range, dissipation range).

(iii) The *temporal properties* of the turbulence. In reality, one expects to find propagating plasma waves which can be damped in a certain way.

In general, all these properties can have an important influence on the energetic particles depending on the transport process which is investigated (e.g. parallel diffusion, perpendicular diffusion, stochastic acceleration) and the considered parameters (e.g. particle energy). In the current paper, we focus on the relevance of wave propagation effects on spatial diffusion of the charged particles. Our aim is to compute parallel and perpendicular diffusion parameters analytically and numerically by using the aforementioned tools.

Alfvén waves (see Alfvén 1942) are a certain type of plasma wave and they are regarded as a transient electro-hydro-magnetic phenomena occurring within a magnetized plasma. Their frequencies are well below the ion-cyclotron frequency ($\omega^2 \ll \omega_c^2$) and their propagating direction is parallel with respect to the large-scale

magnetic field. More about this type of plasma wave can be found in Chen (1984) and Schlickeiser (2002).

In this paper, we explore particle diffusion in Alfvénic slab turbulence analytically and numerically. By doing this, we try to achieve the following:

(i) We extend the so-called Unified Non-Linear Transport (UNLT) theory originally derived in Shalchi (2010) to allow the description of particles interacting with propagating plasma waves. Furthermore, we will derive analytically the perpendicular diffusion coefficient based on the aforementioned theory.

(ii) We perform detailed simulations to explore how the different transport parameters depend on parameters such as the rigidity, the magnetic field ratio $\delta B/B_0$, and the Alfvén speed $v_{\rm A}$.

(iii) We compare the analytical results with the simulations to investigate the accuracy and reliability of analytical tools such as the UNLT theory.

The remainder of this paper is organized as follows. In Section 2, we briefly discuss the model of parallel propagating shear Alfvén waves. The corresponding quasi-linear parallel mean free path is calculated in Section 3. In Section 4, we compute the perpendicular diffusion coefficient analytically based on the UNLT theory. Test-particle simulations are performed in Section 5 where we also compare our numerical results with the analytical findings of the previous sections. We end our paper with a short summary and some conclusions in Section 6.

2 THE MODEL OF PARALLEL PROPAGATING SHEAR ALFVÉN WAVES

A key input in analytical and numerical treatments of particle diffusion is a model for the turbulent electric and magnetic fields. The latter fields are described by so-called correlation tensors. The magnetic correlation tensor, for instance, is defined as

$$P_{lm}\left(\boldsymbol{k},t\right)=\left\langle \delta B_l\left(\boldsymbol{k},t\right)\delta B_m^*\left(\boldsymbol{k},0\right)\right\rangle, \tag{1}$$

where we have used the ensemble average operator $\langle\cdots\rangle$. Often it is assumed that all tensor components have the same temporal behaviour and, thus, one can write

$$P_{lm}\left(\boldsymbol{k},t\right)=P_{lm}\left(\boldsymbol{k}\right)\Gamma\left(\boldsymbol{k},t\right) \tag{2}$$

with the so-called dynamical correlation function $\Gamma\left(\boldsymbol{k},t\right)$ and the magnetostatic tensor $P_{lm}\left(\boldsymbol{k}\right)$. A similar tensor can be defined for electric fields (see, e.g. Schlickeiser 2002). To achieve a certain simplification, we consider only pure magnetic turbulence and, therefore, we only discuss and implement the magnetic correlation tensor.

2.1 The slab model

In the current paper, we employ the so-called slab model in which by definition the turbulent magnetic field depends only on the coordinate along the mean magnetic field (in our case it is the z-axis). In this special case, the static correlation tensor defined above has the form

$$P_{lm}\left(\boldsymbol{k}\right)=g\left(k_{\parallel}\right)\frac{\delta\left(k_{\perp}\right)}{k_{\perp}}\delta_{lm}\quad\text{with}\quad l,m=x,y, \tag{3}$$

where we have used the *Dirac delta* $\delta(z)$, the *Kronecker delta* δ_{lm}, and the one-dimensional spectrum of the slab modes $g(k_{\parallel})$. Below, we specify the latter spectrum. We also like to emphasize that tensor components with $l=z$ or $m=z$ have to be zero due to the solenoidal constraint.

2.2 Parallel propagating shear Alfvén waves

In order to obtain a complete model for the magnetic correlation tensor, we also have to specify the dynamical correlation function. In general, one could assume that (see, e.g. Schlickeiser 2002)

$$\Gamma\left(\boldsymbol{k},t\right)=\mathrm{e}^{-\mathrm{i}\omega t-\gamma t}. \tag{4}$$

The wavenumber-dependent function $\omega=\omega(\boldsymbol{k})$ describes wave propagation effects and the function γ describes damping effects (e.g. plasma wave damping). More details concerning different plasma waves and damping effects can be found in the literature (see, e.g. Bieber et al. 1994; Schlickeiser 2002; Shalchi et al. 2006). In this paper, we only consider undamped waves and, thus, we set $\gamma=0$. For the dispersion relation, we employ the model of parallel propagating shear Alfvén waves where we have by definition

$$\omega=jv_{\rm A}k_{\parallel}\quad\text{with}\quad j=\pm1. \tag{5}$$

In the latter equation, we have used again the Alfvén speed $v_{\rm A}$. The parameter j is used to track the wave direction ($j=+1$ is used for forward and $j=-1$ for backward to the ambient magnetic field propagating Alfvén waves). A lot of studies have addressed the direction of propagation of Alfvénic turbulence (see, e.g. Bavassano 2003). In general, one would expect that closer to the sun the most waves should propagate forward and far away from the sun the wave intensities should be equal for both directions.

2.3 Neglecting electric fields

In the current paper, we investigate particle diffusion in magnetic turbulence. However, we take into account wave propagation effects and, therefore, our turbulence model is dynamical. It is well known due to Maxwell's equations that time-dependent magnetic fields automatically means that electric fields do exist as well (see, e.g. Schlickeiser 2002). To include turbulent electric fields in analytical work and test-particle simulations is difficult. Therefore, we neglect electric fields throughout the whole paper. The importance of electric field for spatial diffusion depends on the parameter $\epsilon=v_{\rm A}/v$. If the latter parameter is small electric fields should be negligible (see again Schlickeiser 2002) and our approach should be valid. If $\epsilon\gg1$, however, electric fields could be important and in this parameter regime our results are eventually no longer valid. Since we want to test theories such as QLT and the UNLT theory, we also consider the case of large ϵ. Our analytical and numerical results can be compared with each other because in both cases we neglect electric fields. We like to emphasize, however, that our results for $\epsilon\gg1$ could be unphysical.

3 THE QUASI-LINEAR PARALLEL MEAN FREE PATH

A standard tool in diffusion theory is QLT originally developed by Jokipii (1966). Although QLT is problematic in the general case, it should work well for parallel diffusion in slab turbulence (see, e.g. Shalchi 2009, for a review). In the current section, we derive analytical expressions for the parallel mean free path. Such calculations are based on the well-known quasi-linear approach (see, e.g. Schlickeiser 2002 for a review).

The parallel spatial diffusion coefficient $\kappa_\parallel$ is given as an integral over the inverse pitch-angle Fokker–Planck coefficient $D_{\mu\mu}(\mu)$ (see, e.g. Earl 1974)

$$\kappa_\parallel = \frac{v\lambda_\parallel}{3} = \frac{v^2}{8}\int_{-1}^{+1} \mathrm{d}\mu\, \frac{(1-\mu^2)^2}{D_{\mu\mu}(\mu)}. \tag{6}$$

Here, we have used the pitch-angle cosine μ and the particle speed v. Instead of the diffusion coefficient $\kappa_\parallel$ one can compute the parallel mean free path $\lambda_\parallel = 3\kappa_\parallel/v$.

For slab turbulence the pitch-angle Fokker–Planck coefficient has the form (see, e.g. Schlickeiser 2002)

$$D_{\mu\mu}(\mu) = \frac{\pi^2\Omega^2(1-\mu^2)}{B_0^2}\int_{-\infty}^{\infty} \mathrm{d}k_\parallel\, g(k_\parallel)\left(1-\frac{\mu\omega}{vk_\parallel}\right)^2 \times\left[\delta\left(v\mu k_\parallel-\omega+\Omega\right)+\delta\left(v\mu k_\parallel-\omega-\Omega\right)\right], \tag{7}$$

where we have used the one-dimensional spectrum of the slab modes $g(k_\parallel)$ and the unperturbed gyro-frequency Ω. All other parameters are explained above. By specifying the turbulence model, and by combining equation (7) with (6) one can compute the parallel spatial diffusion coefficient. This is done in the following.

3.1 A pure magnetic scenario

The term $(\mu\omega)/(vk_\parallel)$ in equation (7) comes due to electric fields which are taken into account in Schlickeiser (2002). In the current paper, we only simulate pure magnetic turbulence, and because of consistency, we have to neglect this term here as well. For parallel propagating shear Alfvén waves, we have to use equation (5) and therewith equation (7) becomes

$$D_{\mu\mu}(\mu) = \frac{\pi^2\Omega^2(1-\mu^2)}{B_0^2}\int_{-\infty}^{\infty} \mathrm{d}k_\parallel\, g(k_\parallel) \times\left\{\delta\left[(v\mu-jv_\mathrm{A})k_\parallel+\Omega\right]+\delta\left[(v\mu-jv_\mathrm{A})k_\parallel-\Omega\right]\right\}. \tag{8}$$

Now we employ the relation $\delta(az) = \delta(z)/|a|$ and perform the wavenumber integral to get

$$D_{\mu\mu}(\mu) = \frac{\pi^2\Omega^2(1-\mu^2)}{B_0^2\,|v\mu-jv_\mathrm{A}|} \times\left[g\left(k_\parallel=-\frac{\Omega}{v\mu-jv_\mathrm{A}}\right)+g\left(k_\parallel=\frac{\Omega}{v\mu-jv_\mathrm{A}}\right)\right]. \tag{9}$$

Since model spectra are usually symmetric $g(k_\parallel) = g(-k_\parallel)$, we finally obtain

$$D_{\mu\mu}(\mu) = \frac{2\pi^2\Omega^2(1-\mu^2)}{B_0^2\,|v\mu-jv_\mathrm{A}|}\, g\left(k_\parallel=\frac{\Omega}{v\mu-jv_\mathrm{A}}\right). \tag{10}$$

In the following, we use the spectrum

$$g^{\mathrm{slab}}(k_\parallel) = \frac{C(s)}{2\pi}\delta B_{\mathrm{slab}}^2 l_{\mathrm{slab}}\frac{1}{\left[1+(k_\parallel l_{\mathrm{slab}})^2\right]^{s/2}}, \tag{11}$$

where we have used

$$C(s) = \frac{\Gamma\left(\frac{s}{2}\right)}{2\sqrt{\pi}\,\Gamma\left(\frac{s-1}{2}\right)}. \tag{12}$$

Furthermore, we have used the inertial range spectral index s, the bendover scale l_{slab}, and the total turbulent magnetic field strength δB_{slab}. This type of spectrum was originally introduced by Bieber et al. (1994) and is frequently used in transport theory. Although Shalchi & Weinhorst (2009) proposed a generalized spectrum, there are some indications that the spectrum (11) is still appropriate for slab turbulence (see Matthaeus et al. 2007).

By combining the spectrum (11) with equation (10) and by using the parameters $\epsilon = v_\mathrm{A}/v$ and $R = R_\mathrm{L}/l_{\mathrm{slab}}$ (here we have used the unperturbed Larmor radius $R_\mathrm{L} = v/\Omega$), the pitch-angle Fokker–Planck coefficient becomes

$$D_{\mu\mu}(\mu) = \pi C(s)(1-\mu^2)\frac{\Omega^2}{v}l_{\mathrm{slab}}\frac{\delta B_{\mathrm{slab}}^2}{B_0^2} \times\frac{|\mu-j\epsilon|^{s-1}}{\left[|\mu-j\epsilon|^2+R^{-2}\right]^{s/2}}. \tag{13}$$

To simplify the latter formula, we consider two different limits.

3.2 The limit $\epsilon \ll 1$

In the case considered here, equation (13) becomes

$$D_{\mu\mu}(\mu) = \pi C(s)(1-\mu^2)\frac{v}{l_{\mathrm{slab}}}R^{s-2}\frac{\delta B_{\mathrm{slab}}^2}{B_0^2} \times\frac{|\mu|^{s-1}}{\left[(\mu R)^2+1\right]^{s/2}}. \tag{14}$$

The latter result corresponds to the well-known magnetostatic limit (see, e.g. equation 3.37 in Shalchi 2009).

3.3 The limit $\epsilon \gg 1$

If $\epsilon \gg 1$, we can approximate $|\mu - j\epsilon| \approx \epsilon$. In this limit, equation (13) becomes

$$D_{\mu\mu}(\mu) = \pi C(s)(1-\mu^2)\frac{v}{l_{\mathrm{slab}}}R^{s-2}\frac{\delta B_{\mathrm{slab}}^2}{B_0^2} \times\frac{\epsilon^{s-1}}{\left[(\epsilon R)^2+1\right]^{s/2}}. \tag{15}$$

We like to note that this limit is questionable because in this limit different physical effects such as electric fields could be important as described in Schlickeiser (2002).

3.4 The parallel mean free path for $\epsilon \ll 1$

Now, we compute the parallel mean free path for the limit $\epsilon \to 0$. In this case, we can use the magnetostatic limit derived before (see, e.g. equation 3.39 of Shalchi 2009) which is given by

$$\frac{\lambda_\parallel}{l_{\mathrm{slab}}} = \frac{3}{8\pi C(s)}\frac{B_0^2}{\delta B_{\mathrm{slab}}^2}R^{2-s} \times\left[\frac{2}{2-s}\,{}_2F_1\left(1-s/2,-s/2;2-s/2;-R^2\right) -\frac{2}{4-s}\,{}_2F_1\left(1-s/2,-s/2;3-s/2;-R^2\right)\right], \tag{16}$$

where we have used the *hypergeometric function* ${}_2F_1(a, b; c; z)$. The latter formula can be simplified by considering two limits.

3.4.1 *The limit $R \ll 1$*

In this case, we can use equation 3.41 of Shalchi (2009) and the parallel mean free path becomes

$$\frac{\lambda_\parallel}{l_{\rm slab}} = \frac{3}{2\pi(2-s)(4-s)C(s)} \frac{B_0^2}{\delta B_{\rm slab}^2} R^{2-s} \tag{17}$$

with the well-known behaviour $\lambda_\parallel \sim R^{2-s}$.

3.4.2 *The limit $R \gg 1$*

In this case, we can use equation 3.42 of Shalchi (2009) to obtain

$$\frac{\lambda_\parallel}{l_{\rm slab}} = \frac{3}{16\pi C(s)} \frac{B_0^2}{\delta B_{\rm slab}^2} R^2 \tag{18}$$

corresponding to the typical $\lambda_\parallel \sim R^2$ behaviour for high rigidities R.

3.5 The parallel mean free path for $\epsilon \gg 1$

In this limit, equation (15) has to be combined with formula (6) to find

$$\frac{\lambda_\parallel}{l_{\rm slab}} = \frac{1}{2\pi C(s)} \frac{B_0^2}{\delta B_{\rm slab}^2} R^{2-s} \epsilon^{1-s} \left[(\epsilon R)^2 + 1\right]^{s/2}. \tag{19}$$

Again, we can identify two different transport regimes.

3.5.1 *The limit $\epsilon R \ll 1$*

In this case, we find that

$$\frac{\lambda_\parallel}{l_{\rm slab}} = \frac{1}{2\pi C(s)} \frac{B_0^2}{\delta B_{\rm slab}^2} R^{2-s} \epsilon^{1-s}. \tag{20}$$

Since we have assumed $s > 1$ ($s = 5/3$ can be seen as standard value for the inertial range spectral index), the parallel mean free path decreases with increasing ϵ in this regime.

3.5.2 *The limit $\epsilon R \gg 1$*

Here, we find that equation (19) yields

$$\frac{\lambda_\parallel}{l_{\rm slab}} = \frac{1}{2\pi C(s)} \frac{B_0^2}{\delta B_{\rm slab}^2} R^2 \epsilon \tag{21}$$

and the parallel mean free path is directly proportional to the parameter ϵ. In Section 5, we will compare the different results derived above with test-particle simulations.

4 THE PERPENDICULAR MEAN FREE PATH BASED ON UNLT THEORY

The UNLT theory provides a non-linear integral equation for the perpendicular diffusion coefficient. In Shalchi (2011a), the theory was extended to allow for dynamical turbulence. In this case, the dynamical correlation function was an exponential function with real argument (corresponding to $\omega = 0$ and $\gamma \neq 0$ in equation (4) of the current paper). In the current section, we consider for the first time the UNLT theory for the case of propagating plasma waves and we derive analytical expressions for the perpendicular diffusion coefficient based on that theory. We can replace the dynamical turbulence model considered in Shalchi (2011a) by the model of undamped propagating plasma waves by using the formal replacement $\omega \to {\rm i}\omega$.

Furthermore, the real part has to be taken and the UNLT theory becomes in this case

$$\kappa_\perp = \frac{a^2 v^2}{3B_0^2} \Re \int {\rm d}^3 k \, \frac{P_{xx}(\boldsymbol{k})}{{\rm i}\omega + F(\boldsymbol{k}) + (4/3)\kappa_\perp k_\perp^2 + v/\lambda_\parallel}, \tag{22}$$

where we have used

$$F(\boldsymbol{k}) = \frac{(2vk_\parallel/3)^2}{{\rm i}\omega + (4/3)\kappa_\perp k_\perp^2}. \tag{23}$$

The parameters used here were already used above except the parameter a. The latter parameter is related to the probability that particles follow magnetic field lines. It is still unclear what the value of that parameter really is in the general case (see, e.g. Matthaeus et al. 2003; Shalchi & Dosch 2008). However, for slab turbulence we expect that particles follow field lines and, therefore, we assume $a = 1$. If the UNLT theory is used in the current paper, we always use this value.

In the following, we employ the slab model (3) and equation (22) becomes

$$\kappa_\perp = 4\pi \frac{a^2 v^2}{3B_0^2} \Re \int_0^\infty {\rm d}k_\parallel \, \frac{g\left(k_\parallel\right)}{{\rm i}\omega + F(k_\parallel) + v/\lambda_\parallel} \tag{24}$$

with

$$F(\boldsymbol{k}) = -{\rm i}\frac{\left(2vk_\parallel\right)^2}{9\omega}. \tag{25}$$

Easily, one can take the real part to find

$$\kappa_\perp = 4\pi \frac{a^2 v^2}{3B_0^2} \frac{v}{\lambda_\parallel} \int_0^\infty {\rm d}k_\parallel \, \frac{g\left(k_\parallel\right)}{v^2/\lambda_\parallel^2 + \left[\omega - \left(2vk_\parallel/3\right)^2/\omega\right]^2}. \tag{26}$$

To proceed, we use the model of parallel propagating shear Alfvén waves (5) and introduce the function

$$A = \left| j\epsilon - \frac{4}{9j\epsilon} \right| = \left| \epsilon - \frac{4}{9\epsilon} \right| \tag{27}$$

with $\epsilon = v_{\rm A}/v$ to find

$$\kappa_\perp = 4\pi \frac{a^2 v^2}{3B_0^2} \frac{v}{\lambda_\parallel} \int_0^\infty {\rm d}k_\parallel \, \frac{g\left(k_\parallel\right)}{v^2/\lambda_\parallel^2 + v^2 A^2 k_\parallel^2}. \tag{28}$$

To proceed, we use the spectrum used in Shalchi (2014):

$$g^{\rm slab}(k_\parallel) = \frac{1}{4\pi^2} l_{\rm slab} \delta B_{\rm slab}^2 \frac{1}{1 + \left(k_\parallel l_{\rm slab}\right)^2}. \tag{29}$$

This spectrum is a special case of the more general form (11). Spectrum (29) corresponds to the model (11) if we set $s = 2$. A more realistic value for the inertial range spectral index would be $s = 5/3$ (see Kolmogorov 1941). However, the exact value of the parameter s is not important if it comes to the perpendicular diffusion coefficient (see, e.g. Shalchi 2013b, 2014 for more details).

With this form of the spectrum, equation (28) becomes

$$\kappa_\perp = \frac{a^2 v^2}{3\pi B_0^2} l_{\rm slab} \delta B_{\rm slab}^2 \frac{v}{\lambda_\parallel} \times \int_0^\infty {\rm d}k_\parallel \, \frac{1}{v^2/\lambda_\parallel^2 + v^2 A^2 k_\parallel^2} \frac{1}{1 + \left(k_\parallel l_{\rm slab}\right)^2}. \tag{30}$$

Now, we use the perpendicular mean free path $\lambda_\perp = 3\kappa_\perp/v$ and the integral transformation $x = k_\parallel l_{\rm slab}$. Furthermore, we introduce

$$B = \frac{l_{\rm slab}}{\lambda_\parallel A} \tag{31}$$

to write

$$\lambda_\perp/l_{\rm slab} = a^2 \frac{\delta B^2_{\rm slab}}{B_0^2} \frac{l_{\rm slab}}{\pi A^2 \lambda_\parallel} \int_0^\infty {\rm d}x \; \frac{1}{B^2+x^2} \frac{1}{1+x^2}. \tag{32}$$

According to Gradshteyn & Ryzhik (2000), the integral yields

$$\int_0^\infty {\rm d}x \; \frac{1}{B^2+x^2} \frac{1}{1+x^2} = \frac{\pi}{2B} \frac{1}{1+B}. \tag{33}$$

Note that B was defined as a positive real number. Therefore, the perpendicular mean free path can finally be written as

$$\lambda_\perp/l_{\rm slab} = \frac{1}{2} a^2 \frac{\delta B^2_{\rm slab}}{B_0^2} \frac{1}{A} \frac{1}{1+B}. \tag{34}$$

By using equations (27) and (31), the latter equation becomes

$$\lambda_\perp/l_{\rm slab} = \frac{1}{2} a^2 \frac{\delta B^2_{\rm slab}}{B_0^2} \frac{1}{\left|\epsilon^2 - 4/9\right|/\epsilon + l_{\rm slab}/\lambda_\parallel}. \tag{35}$$

The latter equation can easily be used to compute the perpendicular mean free path versus the parallel mean free path for certain values of ϵ. Below, we consider different limits/cases to achieve a further simplification of the latter formula.

In Shalchi (2014), the perpendicular mean free path was calculated by evaluating the UNLT theory for a dynamical turbulence model, where $\omega = 0$ but $\gamma \neq 0$. For slab turbulence, a similar formula was obtained there (compare with equation 20 of Shalchi 2014). However, the formula derived in the aforementioned paper is different compared to equation (35) for the general case. Therefore, we conclude that wave propagating effects (described by the dispersion relation ω) and damping effects (described by the parameter γ) influence the perpendicular diffusion coefficient in a different way.

In Shalchi, Bieber & Matthaeus (2004), the perpendicular mean free path was calculated for the same turbulence model considered in the current paper, namely the model of Alfvénic slab turbulence. However, these authors used the non-linear guiding centre theory of Matthaeus et al. (2003). The results they obtained are very different compared to equation (35) derived above (compare with equation 34 of Shalchi et al. 2004).

4.1 The special case $\epsilon \gg l_{\rm slab}/\lambda_\parallel$ and $\epsilon \gg 2/3$

For $\epsilon \gg 2/3$, equation (35) becomes

$$\lambda_\perp/l_{\rm slab} = \frac{1}{2} a^2 \frac{\delta B^2_{\rm slab}}{B_0^2} \frac{1}{\epsilon + l_{\rm slab}/\lambda_\parallel}. \tag{36}$$

If we additionally assume that $\epsilon \gg l_{\rm slab}/\lambda_\parallel$, the latter formula simplifies to

$$\lambda_\perp/l_{\rm slab} = \frac{1}{2} a^2 \frac{\delta B^2_{\rm slab}}{B_0^2} \frac{1}{\epsilon} \equiv \frac{1}{2} a^2 \frac{\delta B^2_{\rm slab}}{B_0^2} \frac{v}{v_{\rm A}}. \tag{37}$$

According to this result, the perpendicular mean free paths decrease with increasing Alfvén speed.

4.2 The special case $l_{\rm slab}/\lambda_\parallel \gg \epsilon \gg 2/3$

In the case considered here, equation (36) can be combined with the assumption $l_{\rm slab}/\lambda_\parallel \gg \epsilon$ and we find

$$\lambda_\perp/l_{\rm slab} = \frac{1}{2} a^2 \frac{\delta B^2_{\rm slab}}{B_0^2} \lambda_\parallel/l_{\rm slab}. \tag{38}$$

The latter formula is well known as diffusion theory (see, e.g. Shalchi 2013b) and corresponds to the case where the particles interact mainly with ballistic field lines while they propagate diffusively in the parallel direction.

4.3 The special case $4\lambda_\parallel/(9l_{\rm slab}) \gg \epsilon$ and $2/3 \gg \epsilon$

For $\epsilon \ll 2/3$, equation (35) becomes

$$\lambda_\perp/l_{\rm slab} = \frac{1}{2} a^2 \frac{\delta B^2_{\rm slab}}{B_0^2} \frac{1}{4/(9\epsilon) + l_{\rm slab}/\lambda_\parallel}. \tag{39}$$

For $4\lambda_\parallel/(9l_{\rm slab}) \gg \epsilon$, the latter formula becomes

$$\lambda_\perp/l_{\rm slab} = \frac{9}{8} a^2 \frac{\delta B^2_{\rm slab}}{B_0^2} \epsilon = \frac{9}{8} a^2 \frac{\delta B^2_{\rm slab}}{B_0^2} \frac{v_{\rm A}}{v}, \tag{40}$$

which is in agreement with equation 47 of Shalchi, Tautz & Schlickeiser (2007). The latter authors used a compound diffusion model to describe perpendicular diffusion. The case considered here, contains also the magnetostatic limit ($\epsilon = 0$) and we can clearly see that in this limit the perpendicular mean free path becomes $\lambda_\perp = 0$ corresponding to subdiffusive transport.

4.4 The special case $2/3 \gg \epsilon \gg 4\lambda_\parallel/(9l_{\rm slab})$

For $4\lambda_\parallel/(9l_{\rm slab}) \ll \epsilon$, equation (39) becomes

$$\lambda_\perp/l_{\rm slab} = \frac{1}{2} a^2 \frac{\delta B^2_{\rm slab}}{B_0^2} \lambda_\parallel/l_{\rm slab}, \tag{41}$$

in agreement with equation (38).

Below, we compare the analytical results derived above with computer simulations.

5 TEST-PARTICLE SIMULATIONS

In the following, we perform simulations to obtain parallel and perpendicular diffusion coefficients numerically. To simulate the transport of energetic particles, one has to perform three steps. The first is the generation of turbulence. Thereafter, we solve the Newton–Lorentz equation numerically and the third step is the calculation of diffusion coefficients based on the ensemble of obtained particle trajectories.

5.1 Generating the turbulence

To create the turbulence, we use the same method used and described in Hussein & Shalchi (2014). This approach is based on previous work where similar simulations were performed (see, e.g. Michałek & Ostrowski 1996; Tautz 2010a,b) and it can be used to create different models such as slab, two-dimensional, and isotropic turbulence. In the following, we describe this approach for the general case and thereafter we specialize to slab turbulence.

The basic idea is to generate random magnetic fluctuations by the superposition of a large number N_m of plane waves. Compared to Hussein & Shalchi (2014), we include an oscillating factor describing the wave propagation effects following Tautz (2010a) and Tautz & Shalchi (2013). In this case, the turbulent magnetic field vector is calculated through

$$\delta \boldsymbol{B}(x,y,z) = Re \sum_{n=1}^{N_m} A(k_n) \hat{\xi}_n {\rm e}^{{\rm i}[k_n z_n' + \beta_n - \omega(k_n)t]}. \tag{42}$$

$A(k_n)$ is the amplitude function (see below), z_n' is the third component of the vector $\boldsymbol{x}_n'$ defined below, β_n is the random phase angle for each wave mode, and $\hat{\xi}_n$ is the polarization (unit) vector. The latter vector is given by

$$\hat{\xi}_n = \cos(\alpha_n)\hat{e}_{x_n'} + {\rm i}\,\sin(\alpha_n)\hat{e}_{y_n'}, \tag{43}$$

where α_n is the random polarization angle and the unit vectors $\hat{e}_{x'_n}$ and $\hat{e}_{y'_n}$ are given by

$$\hat{e}_{x'_n} = \begin{pmatrix} M_{11} \\ M_{12} \\ M_{13} \end{pmatrix} \quad \text{and} \quad \hat{e}_{y'_n} = \begin{pmatrix} M_{21} \\ M_{22} \\ M_{23} \end{pmatrix}. \tag{44}$$

The elements M_{ij} refer to the three-dimensional rotational matrix

$$\mathbf{M} = \begin{pmatrix} \cos\theta_n \cos\phi_n & \cos\theta_n \sin\phi_n & -\sin\theta_n \\ -\sin\phi_n & \cos\phi_n & 0 \\ \sin\theta_n \cos\phi_n & \sin\theta_n \sin\phi_n & \cos\theta_n \end{pmatrix} \tag{45}$$

and the primed coordinates are obtained by

$$\boldsymbol{x}'_n = \mathbf{M} \cdot \boldsymbol{x}. \tag{46}$$

θ_n and ϕ_n are polar and azimuthal angles, respectively. This representation ensures that the solenoidal constraint $\nabla \cdot \delta \boldsymbol{B} = 0$ (corresponding to $\boldsymbol{k}_n \cdot \hat{\xi}_n = 0$) is satisfied. For isotropic turbulence, for instance, the two angles θ_n and ϕ_n are randomly generated for each summand n. For the slab model used here, however, we set the polar angle $\theta_n = 0$ whereas ϕ_n is still generated randomly. We sum over $N_m = 512$ wave modes to create the turbulence with wave numbers ranging from $k_{\min} l_{\rm slab} = 10^{-7}$ to $k_{\max} l_{\rm slab} = 10^5$.

For the dispersion relation in equation (42), we use $\omega(k_n) = j v_{\rm A} k_n$ with $j = \pm 1$ in agreement with equation (5). As before, the parameter j is equal to ± 1 corresponding to forward and backward moving waves. In the simulations, we assume a 50 per cent/50 per cent contribution from either direction. The wave numbers are logarithmically spaced between a minimum wavenumber $k_{\min} l_{\rm slab}$ and a maximum wavenumber $k_{\max} l_{\rm slab}$ in such a way that $\Delta k_n / k_n$ is constant. For the turbulence spectrum, we use the same model as used for the analytical work, namely equation (11). For the inertial range spectrum index, we use the value $s = 5/3$ in agreement with Kolmogorov's theory of turbulence (see Kolmogorov 1941). The amplitude function is related to the spectrum via $A(k_n) \propto \sqrt{g(k_n)}$. More technical details about the creation of turbulence can be found in Hussein & Shalchi (2014).

5.2 Calculating particle trajectories

By using the turbulence simulations described above in combination with the Newton–Lorentz equation, we can compute particle orbits. Since electric fields are neglected, the Newton–Lorentz equation has the form

$$m\gamma \dot{\boldsymbol{v}} = \frac{q}{c} \boldsymbol{v} \times (\boldsymbol{B}_0 + \delta \boldsymbol{B}), \tag{47}$$

where we have used the particle mass m, the particle charge q, the speed of light c, and the Lorentz factor γ. The turbulent magnetic fields are created anew along the trajectory of each particle. This method saves time and memory space compared to the grid method (see again Hussein & Shalchi 2014 for more details). In the following, several dimensionless parameters are introduced, namely the time $\tau = \Omega t$ and rigidity $R = R_{\rm L} / l_{\rm slab}$. By using these parameters, we solve the following two (coupled) differential equations:

$$\frac{\rm d}{{\rm d}\tau} \frac{\boldsymbol{x}}{l_{\rm slab}} = \boldsymbol{R} \tag{48}$$

and

$$\frac{\rm d}{{\rm d}\tau} \boldsymbol{R} = \boldsymbol{R} \times \left(\hat{e}_{B_0} + \frac{\delta B}{B_0} \hat{e}_{\delta B} \right). \tag{49}$$

The two vectors $\hat{e}_{B_0}$ and $\hat{e}_{\delta B}$ are unit vectors pointing in the direction of the background and turbulent magnetic fields, respectively. By using the dimensionless parameters as described above, the plasma wave dispersion relation (5) becomes

$$\omega(k_n) t = \pm R (v_{\rm A}/v)(k_n l_{\rm slab})(\Omega t). \tag{50}$$

The numerical solver used to integrate equations (48) and (49) is based on a fourth-order *Runge–Kutta method*. The trajectories for 1000 particles were calculated for a maximum (dimensionless) time of $\tau_{\max} = 10^4$ or $\tau_{\max} = 10^5$ as needed.

5.3 Obtaining the different diffusion coefficients

In the previous paragraphs, we described how one can obtain an ensemble of test-particle trajectories. From this ensemble, one can compute transport parameters by using mean square displacements. The quantity which is obtained from the simulations is the so-called *running diffusion coefficient*

$$\kappa_{ii}(t) = \frac{1}{2t} \left\langle (\Delta x_i(t))^2 \right\rangle \tag{51}$$

with $\Delta x_i(t) = x_i(t) - x_i(0)$. The calculation of the diffusion parameters via mean square displacements, however, is not valid if it comes to the drift coefficient(s) κ_{xy} and κ_{yx} (see Shalchi 2011b). From equation (51), the diffusion coefficient can then be obtained by looking at the late time behaviour corresponding to the limit $t \to \infty$ in analytical treatments of the transport. Alternatively, one can compute mean free paths which are related to spatial diffusion coefficients via $\lambda_i = 3\kappa_i / v$.

5.4 Simulation results

We perform the simulations to compute parallel and perpendicular mean free paths. Our aim is to explore how these two parameters depend on the rigidity R, the turbulence strength $\delta B / B_0$, and Alfvén speed $v_{\rm A}$. Our numerical results are listed in Tables 1–4.

In Figs 1 and 2, we show the parallel and perpendicular mean free paths versus the time. One can easily see that diffusive behaviour is obtained for the parallel diffusion coefficient for all considered values of $\epsilon = v_{\rm A}/v$. For the perpendicular diffusion coefficient we find the well-known subdiffusive behaviour if $\epsilon = 0$. As soon as $\epsilon \neq 0$, diffusion is recovered. This conclusion agrees with the results obtained before by Michałek & Ostrowski (1996) and Tautz (2010a).

In Fig. 3, we show the perpendicular mean free path versus the magnetic field ratio $\delta B_0 / B_0$ for $R = 1.0$ and $v_{\rm A}/v = 0.1$. One can easily see that $\lambda_\perp \sim \delta B^2 / B_0^2$ for the considered parameter regime.

Table 1. The simulated mean free paths along and across the mean magnetic field versus the ratio $\epsilon = v_{\rm A}/v$. Here, we have used $R = R_{\rm L}/l_{\rm slab} = 0.1$, $\delta B/B_0 = 1$, and $s = 5/3$.

$v_{\rm A}/v$	0.0	0.01	0.02	0.04	0.06	0.08	0.1	1.0	2	5	10	50	100	10^3	10^4
$\lambda_\parallel / l_{\rm slab}$	2.4	2.5	2.5	2.6	2.6	2.45	2.3	0.58	0.38	0.28	0.28	0.9	1.9	29	73
$\lambda_\perp / l_{\rm slab}$	subdiff.	0.01	0.02	0.04	0.06	0.08	0.1	0.15	0.075	0.04	0.025	0.0065	0.0035	0.0003	7.0×10^{-5}

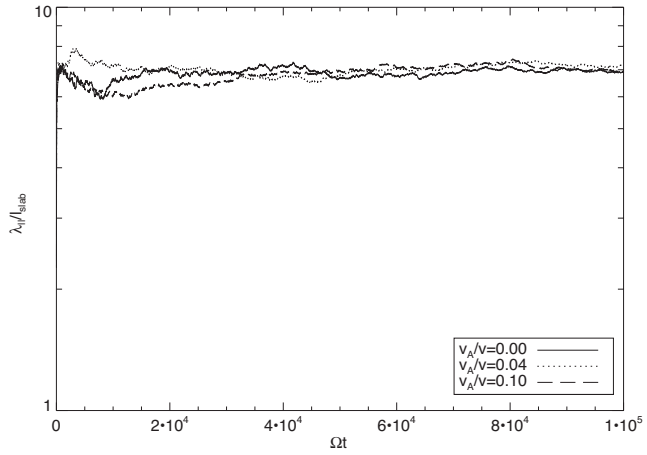

Figure 1. The (running) parallel mean free path $\lambda_\parallel/l_{\rm slab}$ versus the dimensionless time $\tau = \Omega t$. Here, we have set $\delta B/B_0 = 1.0$ and $R = 1.0$ and computed the corresponding transport parameter for three different values of $\epsilon = v_{\rm A}/v$.

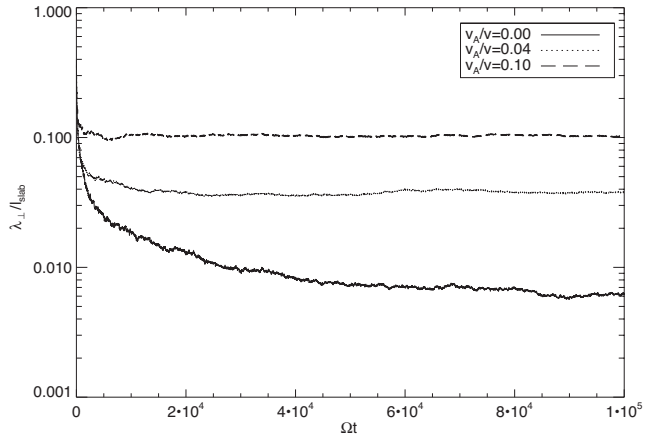

Figure 2. The (running) perpendicular mean free path $\lambda_\perp/l_{\rm slab}$ versus the dimensionless time $\tau = \Omega t$. Here, we have set $\delta B/B_0 = 1.0$ and $R = 1.0$ and computed the corresponding transport parameter for three different values of $\epsilon = v_{\rm A}/v$.

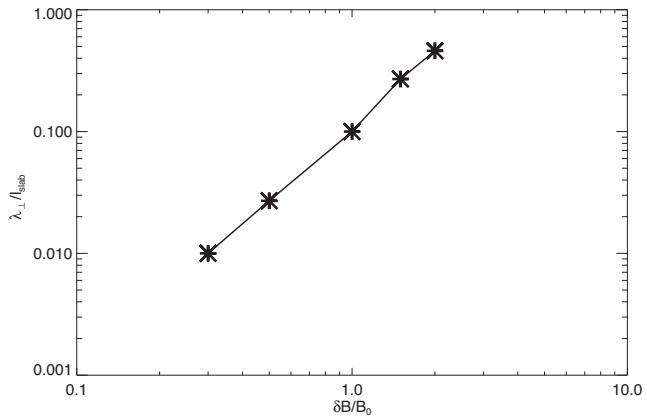

Figure 3. The perpendicular mean free path $\lambda_\perp/l_{\rm slab}$ versus the magnetic field ratio $\delta B_0/B_0$ for $R = 1.0$ and $\epsilon \equiv v_{\rm A}/v = 0.1$. The slope of this graph is very close to 2 confirming the scaling $\lambda_\perp/l_{\rm slab} \sim (\delta B/B_0)^2$ obtained from the UNLT theory.

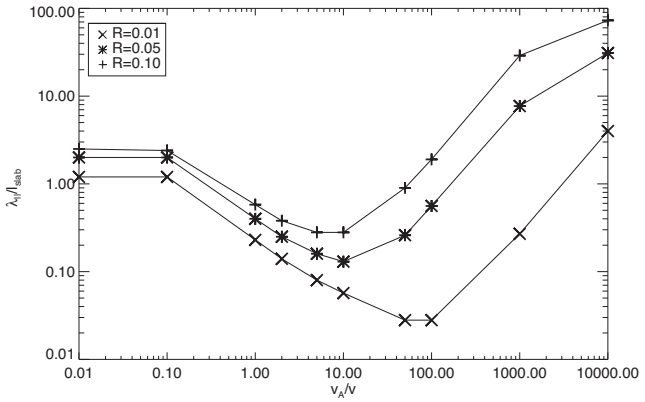

Figure 4. The parallel mean free path $\lambda_\parallel/l_{\rm slab}$ versus $v_{\rm A}/v$ for three different values of the rigidity R and constant $\delta B/B_0 = 1.0$.

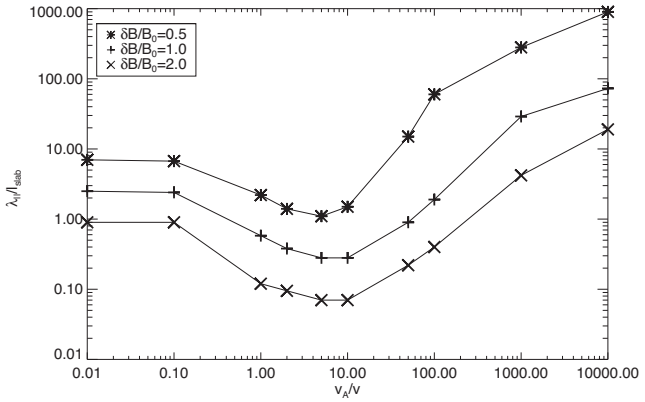

Figure 5. The parallel mean free path $\lambda_\parallel/l_{\rm slab}$ versus $v_{\rm A}/v$ for three different values of $\delta B/B_0$ and constant $R = 0.1$.

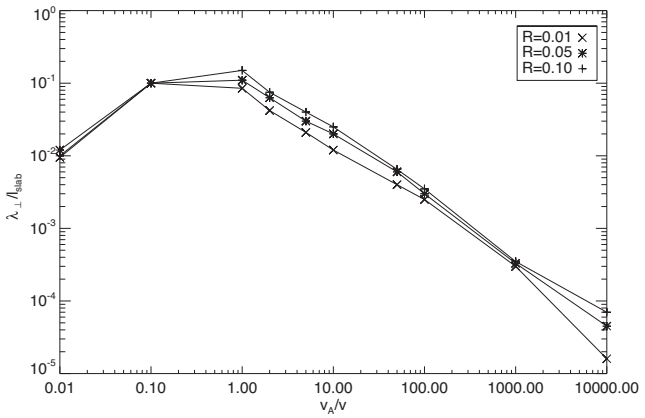

Figure 6. The perpendicular mean free path $\lambda_\perp/l_{\rm slab}$ versus $v_{\rm A}/v$ for three different values of the rigidity R and constant $\delta B/B_0 = 1.0$.

This behaviour is in agreement with the results provided by UNLT theory. We like to emphasize that one can also find a parameter regime where the perpendicular mean free path is directly proportional to the parallel mean free path. Since the latter parameter depends also on the magnetic field ratio, the magnetic field dependence of the perpendicular diffusion coefficient is more complicated in such cases.

In Figs 4–7, we compute the parallel and perpendicular mean free paths versus $\epsilon = v_{\rm A}/v$ for different values of the ratio $\delta B_0/B_0$

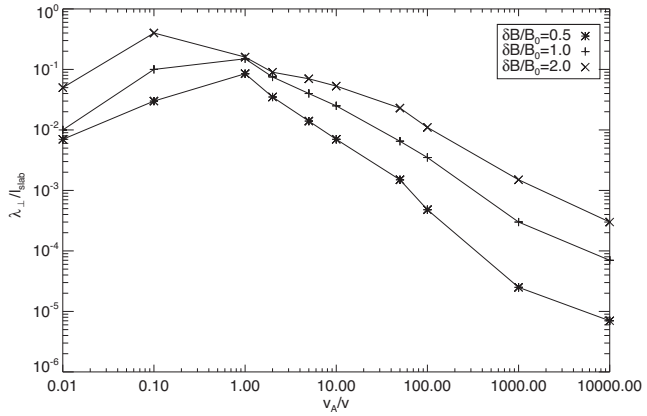

Figure 7. The perpendicular mean free path $\lambda_{\parallel}/l_{\rm slab}$ versus $v_{\rm A}/v$ for three different values of $\delta B/B_0$ and constant $R = 0.1$.

and different magnetic rigidities represented by the parameter $R \equiv R_{\rm L}/l_{\rm slab}$. As shown, the magnetic field ratio as well as the rigidity have a strong influence on the parallel mean free path as expected. The perpendicular mean free path, however, does not explicitly depend on the rigidity for the parameter regimes considered here. Changing the magnetic field ratio does change the perpendicular diffusion parameter as already discussed above.

5.5 Testing analytical predictions

Above, we have shown different numerical results for the case of parallel propagating shear Alfvén waves. In the following, we compare our simulations directly with the analytical results derived in Sections 3 and 4. To calculate the parallel mean free path, we use equations (16) and (19), and for the perpendicular mean free path we employ equation (35). For the latter calculations, we set $a^2 = 1$ as discussed in Section 4.

In Fig. 8, we show the two mean free paths versus the ratio $\epsilon \equiv v_{\rm A}/v$ for $R_{\rm L}/l_{\rm slab} = 0.1$, $\delta B/B_0 = 1$, and $s = 5/3$. According

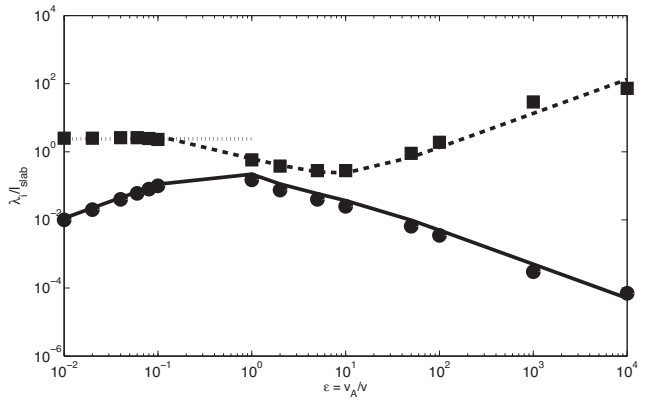

Figure 8. The parallel mean free path and the perpendicular mean free path versus $\epsilon \equiv v_{\rm A}/v$. Here, we have used $R_{\rm L}/l_{\rm slab} = 0.1$, $\delta B^2/B_0^2 = 1$, and $s = 5/3$. Shown are the simulated parallel mean free paths (squares) and the simulated perpendicular mean free path (dots). The theoretical parallel mean free paths are based on QLT and were computed by employing equation (16) for small values of ϵ (dotted line) and equation (19) for large values of ϵ (dashed line), respectively. The theoretical perpendicular mean free paths were calculated by using equation (35) which is based on the UNLT theory (solid line).

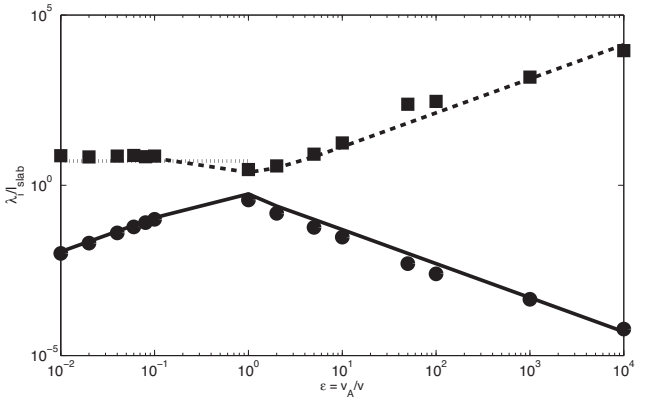

Figure 9. Figure caption is the same as in Fig. 8 but here we have used $R_{\rm L}/l_{\rm slab} = 1.0$.

to this figure, QLT agrees very well with the parallel mean free paths obtained numerically. Furthermore, the simulations confirm the UNLT theory for parallel propagating shear Alfvén waves. In Fig. 9, we provide a similar comparison but we have changed the rigidity from $R_{\rm L}/l_{\rm slab} = 0.1$–$1.0$. For this value of R, QLT and UNLT theory are confirmed also. The results from our test-particle simulations are listed in Tables 1 and 2 to make it easier for the reader to reproduce the figures if required.

In Tables 3 and 4, we have shown more simulations. Here, we employed our code for the cases where $v \approx v_{\rm A}$. In this case, equation (38) should be valid and we expect that $\lambda_{\perp}/\lambda_{\parallel} \approx 0.5$. Our simulations also confirm the UNLT theory for such cases.

6 SUMMARY AND CONCLUSION

In the current paper, we have investigated the interaction of energetic particles with parallel propagating shear Alfvén waves. For the analytical work, we have used QLT to compute the parallel diffusion coefficient. This procedure is well known in diffusion theory (see, e.g. Schlickeiser 2002) and based on the assumption that QLT is valid for parallel transport in slab turbulence (see, e.g. Shalchi 2009). The perpendicular diffusion coefficient is calculated by extending the UNLT theory of Shalchi (2010, 2011a). We have also performed detailed test-particle simulations for the same turbulence model.

In this work, we have achieved the following:

(i) We have derived an integral equation for the perpendicular diffusion coefficient based on UNLT theory (see equations 22 and 23 of this paper). The latter equations were then combined with the slab model of turbulence (see equation 28). For a model spectrum, a simple formula for the perpendicular diffusion coefficient was derived. Equation (35) allows the analytical description of perpendicular transport if the parallel diffusion coefficient is known.

(ii) We used test-particle simulations to explore how parallel and perpendicular diffusion parameters depend on the magnetic rigidity, the magnetic field ratio $\delta B/B_0$, and the Alfvén speed $v_{\rm A}$. Figs 3–7 show our results. This work complements previous numerical work such as the papers by Michałek & Ostrowski (1996), Tautz (2010a), and Tautz & Shalchi (2013).

(iii) We presented a detailed comparison between analytical theory and computer simulations to check our understanding of particle transport in Alfvénic slab turbulence (see Figs 8 and 9). According to this comparison, QLT works very well for parallel transport for this specific turbulence model. This confirmed our expectations.

Table 2. The simulated mean free paths along and across the mean magnetic field versus the ratio $\epsilon = v_A/v$. Here, we have used $R = R_L/l_{slab} = 1.0$, $\delta B/B_0 = 1$, and $s = 5/3$.

v_A/v	0.0	0.01	0.02	0.04	0.06	0.08	0.1	1.0	2	5	10	50	100	10^3	10^4
$\lambda_\parallel/l_{slab}$	7.0	7.4	6.8	7.2	7.5	6.9	7.2	2.9	3.7	8.2	17.5	240	290	1500	9000
$\lambda_\perp/l_{slab}$	subdiff.	0.01	0.02	0.04	0.06	0.08	0.1	0.37	0.15	0.058	0.03	0.005	0.0025	0.000 45	6.0×10^{-5}

Table 3. The simulated mean free paths along and across the mean magnetic field versus the rigidity $R = R_L/l_{slab}$. Here, we have used $\epsilon = v_A/v = 2/3$, $\delta B/B_0 = 1$, and $s = 5/3$.

R	0.0001	0.0005	0.001	0.005	0.01	0.05	0.1
$\lambda_\parallel/l_{slab}$	0.084	0.18	0.25	0.29	0.35	0.53	0.78
$\lambda_\perp/l_{slab}$	0.038	0.08	0.11	0.13	0.15	0.22	0.27
$\lambda_\perp/\lambda_\parallel$	0.45	0.44	0.44	0.45	0.43	0.42	0.35

Table 4. The simulated mean free paths along and across the mean magnetic field versus the rigidity $R = R_L/l_{slab}$. Here, we have used $\epsilon = v_A/v = 1$, $\delta B/B_0 = 1$, and $s = 5/3$.

R	0.0001	0.0005	0.001	0.005	0.01	0.05	0.1
$\lambda_\parallel/l_{slab}$	0.074	0.11	0.13	0.19	0.22	0.33	0.58
$\lambda_\perp/l_{slab}$	0.03	0.044	0.052	0.077	0.085	0.11	0.15
$\lambda_\perp/\lambda_\parallel$	0.41	0.40	0.40	0.41	0.39	0.33	0.26

Furthermore, the perpendicular diffusion coefficient provided by UNLT theory is almost perfectly in coincidence with the numerical work.

Since the validity of QLT in Alfvénic slab turbulence is known, the most important result of the current paper is the fact that UNLT theory agrees with the simulated perpendicular diffusion coefficients for the cases we considered. Though this is not a general proof, this confirms again that UNLT theory is a powerful tool in diffusion theory. The latter theory was already confirmed to be valid for a magnetostatic slab/2D composite model and Goldreich–Sridhar turbulence (see Tautz & Shalchi 2011; Shalchi 2013a).

ACKNOWLEDGEMENTS

MH and AS acknowledge support by the Natural Sciences and Engineering Research Council (NSERC) of Canada and national computational facility provided by WestGrid. We are also grateful to Samar Safi-Harb for providing her CFI-funded computational facilities for code tests and for some of the simulation runs presented here.

REFERENCES

Alania M. V., Wawrzynczak A., Sdobnov V. E., Kravtsova M. V., 2013, Sol. Phys., 286, 561
Alfvén H., 1942, Nature, 150, 405
Bavassano B., 2003, in Velli M., Bruno R., Malara F., eds, AIP Conf. Proc. Vol. 679, Solar Wind Ten: Proceedings of the Tenth International Solar Wind Conference. Am. Inst. Phys., New York, p. 377
Bieber J. W., Matthaeus W. H., Smith C. W., Wanner W., Kallenrode M.-B., Wibberenz G., 1994, ApJ, 420, 294
Chen F., 1984, Sky Telesc., 67, 527
Earl J. A., 1974, ApJ, 193, 231
Engelbrecht N. E., Burger R. A., 2013, ApJ, 779, 158
Gradshteyn I. S., Ryzhik I. M., 2000, Table of Integrals, Series, and Products. Academic Press, New York
Hussein M., Shalchi A., 2014, ApJ, 785, 31
Jokipii J. R., 1966, ApJ, 146, 480
Kolmogorov A. N., 1941, Dokl. Akad. Nauk SSSR, 30, 301
Li G., Shalchi A., Ao X., Zank G., Verkhoglyadova O. P., 2012, Adv. Space Res., 49, 1067
Manuel R., Ferreira S. E. S., Potgieter M. S., 2014, Sol. Phys., 289, 2207
Matthaeus W. H., Qin G., Bieber J. W., Zank G. P., 2003, ApJ, 590, L53
Matthaeus W. H., Bieber J. W., Ruffolo D., Chuychai P., J. Minnie, 2007, ApJ, 667, 956
Michałek G., Ostrowski M., 1996, Nonlinear Process. Geophys., 3, 66
Perrone D. et al., 2013, Space Sci. Rev., 178, 233
Potgieter M. S., Vos E. E., Boezio M., De Simone N., Di Felice V., Formato V., 2014, Sol. Phys., 289, 391
Qin G., Matthaeus W. H., Bieber J. W., 2002, Geophys. Res. Lett., 29, 1048
Schlickeiser R., 2002, Cosmic Ray Astrophysics, Springer, Berlin
Shalchi A., 2009, Nonlinear Cosmic Ray Diffusion Theories, Astrophys. Space Sci. Libr., Vol. 362, Springer, Berlin
Shalchi A., 2010, ApJ, 720, L127
Shalchi A., 2011a, Plasma Phys. Control. Fusion, 53, 074010
Shalchi A., 2011b, Phys. Rev. E, 83, 046402
Shalchi A., 2013a, Ap&SS, 344, 187
Shalchi A., 2013b, ApJ, 774, 7
Shalchi A., 2014, Adv. Space Res., 53, 1024
Shalchi A., Dosch A., 2008, ApJ, 685, 971
Shalchi A., Weinhorst B., 2009, Adv. Space Res., 43, 1429
Shalchi A., Bieber J. W., Matthaeus W. H., 2004, ApJ, 615, 805
Shalchi A., Bieber J. W., Matthaeus W. H., Schlickeiser R., 2006, ApJ, 642, 230
Shalchi A., Tautz R. C., Schlickeiser R., 2007, A&A, 475, 415
Tautz R. C., 2010a, Plasma Phys. Control. Fusion, 52, 045016
Tautz R. C., 2010b, Comput. Phys. Commun., 181, 71
Tautz R. C., Shalchi A., 2011, ApJ, 735, 92
Tautz R. C., Shalchi A., 2013, J. Geophys. Res.: Space Phys., 118, 642
Wang Y., Qin G., Zhang M., 2012, ApJ, 752, 37

This paper has been typeset from a TEX/LATEX file prepared by the author.